Unconventional Ballooning Structures for Toroidal Drift Waves

H. S. Xie[1,*] and Y. Xiao[1,†]

[1] *Institute for Fusion Theory and Simulation, Department of Physics, Zhejiang University, Hangzhou, 310027, People's Republic of China*

(Dated: March 11, 2015)

The conventional ballooning structures for toroidal drift waves peak in the outboard mid-plane of tokamaks. With strong gradients in the pedestal of H-mode plasmas, gyrokinetic simulations are carried out for the trapped electron and ion temperature gradient modes. General unconventional mode structures that can localize at arbitrary poloidal positions or with multiple peaks are found. By solving the eigenvalue problem of a simplified model equation, it is found that series eigen solutions exist. At weak gradient (L-mode), the most unstable solution is usually the ground eigen state, which corresponds to a conventional mode structure. However, at strong gradient (H-mode), the most unstable solutions usually are not the ground eigen state and the mode structures are general. This result implies that the transport properties of H-mode can be significantly different from those of L-mode. [2015-03-11 14:20 rev]

PACS numbers: 52.35.Py, 52.30.Gz, 52.35.Kt

Drift wave turbulence existing universally in magnetized plasmas is believed to be the major cause of anomalous transport[1] in tokamaks. It is crucial to understand the properties of the micro-instabilities that lead to the drift wave turbulence, especially in the high-confinement mode (H-mode) of tokamaks.

In this Letter, we show that the linear properties of two major types of electrostatic micro-instabilities, namely the trapped particle mode (TEM) and ion temperature gradient (ITG) mode, are completely different in the H-mode (strong gradient) and L-mode (weak gradient) stages. With the conventional weak gradient, the mode structures for drift wave instabilities such as the ITG and TEM are of ballooning type, peaking at the outboard mid-plane of the tokamak (c.f., [2–4]). This type of solution has been intensively studied using the ballooning-representation[5, 6] by reducing one 2D eigen mode equation for the drift waves to two 1D eigen mode equations. The most unstable solutions in the ballooning space found in the past have usually the ballooning-angle parameter $\vartheta_k = 0$[7], which corresponds to the solution localized at the outside mid-plane, i.e., $\theta_p = 0$ in our notation, where θ_p is defined as the peaking poloidal angle for the mode structure. For this reason, many local eigenvalue codes such as HD7[8] assume implicitly $\vartheta_k = 0$. The unconventional eigen modes with $\vartheta_k \neq 0$ have been recently discovered in the strong gradient parameter regime. Typically, $|\theta_p| \simeq$ or $< \pi/2$ have been shown to exist[3, 4, 9, 10]. In this work, we find the most general unconventional eigen mode structures from first principle gyrokinetic simulations. The underlying physics is also explained and it has important implications for turbulent transport.

We first obtain linear electrostatic results from gyrokinetic particle simulation using the GTC code[11, 12] with single toroidal mode number n. The simulation parameters and profiles are similar to that of the recent H-mode experiments of the HL-2A tokamak[13]: toroidal magnetic field $B_0 = 1.35T$, minor radius $a = 40cm$, major radius $R_0 = 165cm$, safety factor $q = 2.5 - 3.0$, magnetic shear $s = 0.3 - 1.0$, $R_0/L_T = 80 - 160$ with $T_e(r) = T_i(r)$, and $n_e(r) = n_i(r)$. L_n and L_T are density and temperature gradient scale length. We start with $\eta = L_n/L_T \simeq 1.0$ for simplicity. Collisions are included in some cases but shown little influence to the general results. Under these parameters, no instability or only weakly unstable mode can be found when the electrons are adiabatical. Thus, the major instability for these simulation parameters is the trapped electron mode.

These TEM simulations show that both conventional and unconventional ballooning mode structures can exist for various temperature gradients and toroidal mode numbers ($n = 5 - 30$) , as shown by Fig.1. The novel features include: a). the mode can have anti-ballooning structure (i.e., $|\theta_p| > \pi/2$, e.g., Fig.1g); b). the mode can have multiple peaks (e.g., Fig.1b). Considering that the trapped particles are usually located at the low magnetic field side, i.e., the outboard side, the anti-ballooning structures of TEM are not expected. The 3D mode structure of the electrostatic potential can be represented by the Fourier series $\delta\phi(r,\theta,\zeta) = e^{in\zeta}\sum_m \delta\phi_m(r)e^{-im\theta}$, where m is poloidal mode number. To explore the formation of these different eigenmode structures, we compute the $\delta\phi_m(r)$ for several typical conventional and unconventional mode structures, as shown in Fig.2. For the conventional ballooning structure, the poloidal eigen modes $\delta\phi_m(r)$ are almost radially symmetric (Gaussian-like) and positive in amplitude. And, $\delta\phi_m$ has a large overlap with $\delta\phi_{m+1}$, i.e., $\delta\phi_m \simeq \delta\phi_{m+1}$. However, for the unconventional structures, the poloidal eigen modes $\delta\phi_m(r)$ can be radially either symmetric or asymmetric, and the amplitude for each symmetric mode can be either positive or negative, as shown by Fig. 2b, c and d.

*Email: huashengxie@gmail.com

†Email (Corresponding author): yxiao@zju.edu.cn

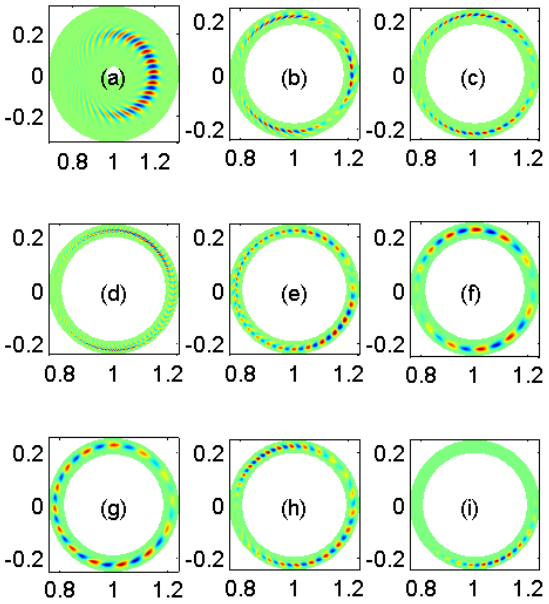

FIG. 1: Conventional (a) and unconventional (b-i) ballooning structures of electrostatic potential for TEM observed in GTC simulation, where (a) uses weak gradient L-mode (Cyclone base case[2]) parameter and (b)-(i) use strong gradient H-mode parameters. Collisions are only included in (e) and (g).

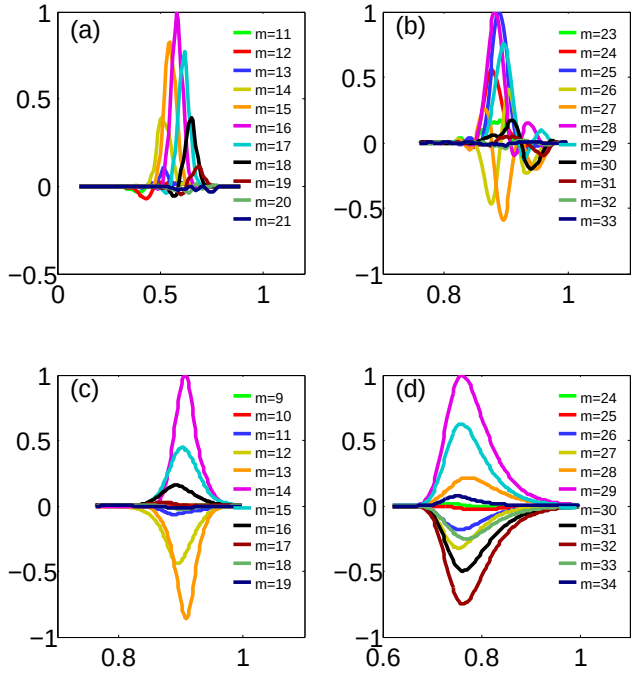

FIG. 2: The real part of Fourier $\delta\phi_m(r)$ for conventional and unconventional mode structures. The corresponding poloidal cross section mode structures of (a)-(d) are taken from Fig.1 (a), (b), (g) and (i), respectively.

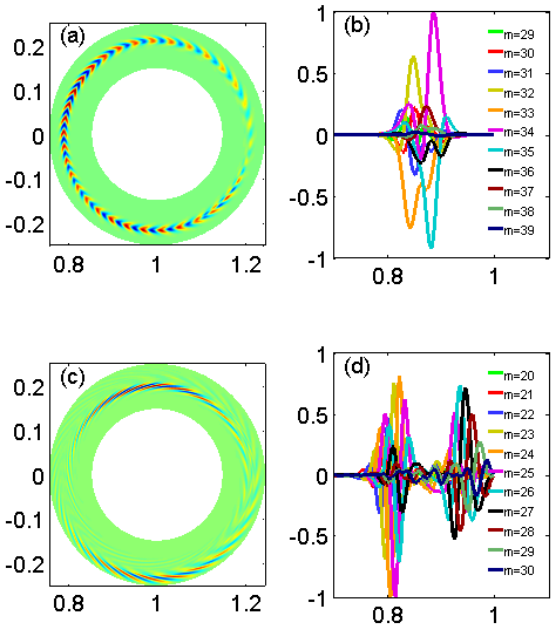

FIG. 3: unconventional ITG mode structures in GTC. (a & b) Anti-ballooning structure. (c & d) Two modes co-exist (or, one mode with two radius peaks) at different radius positions. One has $\theta_p \simeq \pi/2$ and another has $\theta_p \simeq -\pi/2$.

Next we consider ITG mode by reducing the density gradient. To completely exclude the contribution of the kinetic electrons, we use adiabatic electrons in the simulations. It is found that the preceding unconventional mode structures still exist and exhibit even more structural variations. For example, the anti-ballooning structure is found for this ITG simulation, as is shown in Fig.3a&b. Actually, the mode structure with global profiles and multi modes coexisting in the initial value simulation can be even more complicated. For example, two modes with similar growth rates can be excited in different radial locations, as shown in Fig.3c&d. Multi modes coexist with close peaking positions in the initial value simulation can also lead to $\theta_p = \theta_p(t)$, i.e., rotate poloidally with time. Thus, these unconventional mode structures are not limited to TEM and can be common for drift waves.

These unconventional linear behaviors can be understood from the following eigenmode analysis. We start with the ITG eigen mode equation[4, 6]

$$\Big[\rho_i^2\frac{\partial^2}{\partial x^2} - \frac{\sigma^2}{\omega^2}\Big(\frac{\partial}{\partial\theta} + ik_\theta s x\Big)^2 - \frac{2\epsilon_n}{\omega}\Big(\cos\theta + \frac{i\sin\theta}{k_\theta}\frac{\partial}{\partial x}\Big) - \frac{\omega-1}{\omega+\eta_s} - k_\theta^2\rho_i^2\Big]\delta\phi(x,\theta) = 0, \quad (1)$$

where $\sigma = \epsilon_n/(qk_\theta\rho_i)$, $\epsilon_n = L_n/R_0$, $\eta_s = 1+\eta_i$, $x = r-r_s$ and the poloidal wave number $k_\theta = nq/r$. Eq.(1) can be derived from the gyrokinetic theory with adiabatic

electron assumption. The corresponding 1D eigen mode equation in the ballooning space is

$$\Big\{\frac{\sigma^2}{\omega^2}\frac{d^2}{d\vartheta^2}+k_\theta^2\rho_i^2[1+s^2(\vartheta-\vartheta_k)^2]+\frac{2\epsilon_n}{\omega}[\cos\vartheta +s(\vartheta-\vartheta_k)\sin\vartheta]+\frac{\omega-1}{\omega+\eta_s}\Big\}\delta\hat{\phi}(\vartheta,\vartheta_k)=0, \quad (2)$$

where ϑ_k is the ballooning-angle parameter, which represents an as yet undetermined radial wavenumber[6]. Using the Fourier basis $\delta\phi(x,\theta)=\sum_m u_m e^{-im\theta}$, Eq.(1) can be rewritten as the 2D eigenmode equation

$$k_\theta^2\rho_i^2 s^2\frac{\partial^2 u_m}{\partial z^2}+\frac{\sigma^2}{\omega^2}(z-m)^2u_m-\frac{\epsilon_n}{\omega}\Big[\Big(1-s\frac{\partial}{\partial z}\Big)u_{m-1} +\Big(1+s\frac{\partial}{\partial z}\Big)u_{m-1}\Big]-\Big(\frac{\omega-1}{\omega+\eta_s}+k_\theta^2\rho_i^2\Big)u_m=0, \quad (3)$$

where $z=k_\theta s x$. To solve the eigenvalue problem of Eq.(3), only several m modes need to be kept.

With suitable approximations, both Eqs.(2) and (3) can be reduced to the Weber equation $u''+(bx^2+a)u=0$, which has solutions with the eigenvalues $a(\omega)=i(2l+1)\sqrt{b(\omega)}$ and eigenfunctions $u(x)=H_l(i\sqrt{b}x)e^{-ibx^2/2}$, where H_l is l-th Hermite polynomial and $l=0,1,2,...$, which represent a series eigenstates. With the original equations, i.e., Eqs.(2) and (3), which can only be solved numerically, the eigenstates take a more complicated form.

Eqs.(2) and (3) can be solved numerically by transforming it to a matrix eigenvalue problem as $\omega^3\boldsymbol{M}_3\boldsymbol{X}+\omega^2\boldsymbol{M}_2\boldsymbol{X}+\omega\boldsymbol{M}_1\boldsymbol{X}+\boldsymbol{M}_0\boldsymbol{X}=0$. We use finite difference to discretize the system, which yields sparse matrices for $\boldsymbol{M}_i$ $(i=0,1,2,3)$. Using the companion matrix method, the nonlinear eigenvalue problem can be transformed to a standard eigenvalue problem as $\boldsymbol{AY}=\omega\boldsymbol{BY}$, where $\boldsymbol{Y}=[\boldsymbol{X}_1,\boldsymbol{X}_2,\boldsymbol{X}_3]\equiv[\boldsymbol{X},\omega\boldsymbol{X},\omega^2\boldsymbol{X}]$, $\boldsymbol{A}=[\boldsymbol{O},\boldsymbol{I},\boldsymbol{O};\boldsymbol{O},\boldsymbol{O},\boldsymbol{I};-\boldsymbol{M}_0,-\boldsymbol{M}_1,-\boldsymbol{M}_2]$, $\boldsymbol{B}=[\boldsymbol{I},\boldsymbol{O},\boldsymbol{O};\boldsymbol{O},\boldsymbol{I},\boldsymbol{O};\boldsymbol{O},\boldsymbol{O},\boldsymbol{M}_3]$, and $\boldsymbol{I}$ and $\boldsymbol{O}$ are unit and null matrix respectively. Thus all the solutions of this eigen system can be obtained (c.f., [14] for details of similar treatment). The advantage of this method is that it can show the complete set solutions of the discrete eigen system and help us to understand the distribution of eigenvalues in the complex plane. The solution in Refs.[3, 4] using iterative solver is actually just one of the solutions obtained here and may not be the most unstable or most important, which depends heavily on the initial guess. This companion matrix method has been verified by comparing the numerical solutions with that from the shooting method and the analytical solution whenever it can be found.

By solving Eq.(2) in the 1D ballooning space, the unconventional ballooning structures occur when either the most unstable solution is not the ground eigen state ($l\neq 0$), or the ballooning angle $\vartheta_k\neq 0$. Both of these two conditions can be met in the strong gradient regime. The most unstable solution with $\vartheta_k\neq 0$ has been discussed by others (c.f., [9, 15]). Here we focus on the unconventional ballooning structure caused by the non-ground

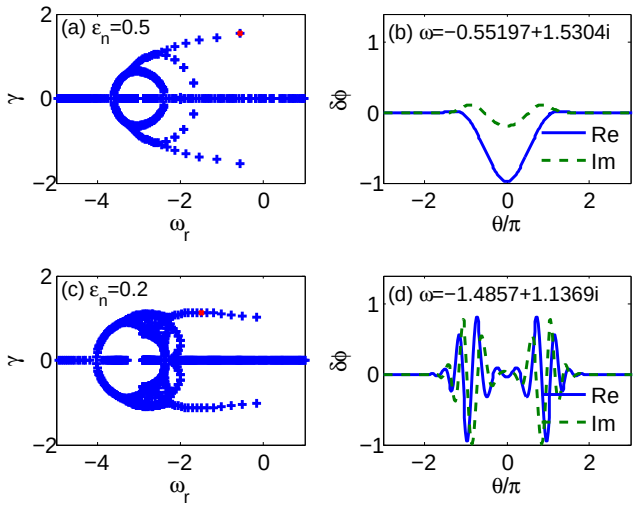

FIG. 4: In Eq.(2), series solutions exist. For weak gradient ($\epsilon_n=0.5$), the most unstable solution is the ground state (a&b), which is the conventional ballooning structure. For strong gradient ($\epsilon_n=0.2$), the most unstable solution is not the ground state (c&d), which represents the unconventional ballooning structure.

eigen state. The following parameters are used to solve Eq.(2): $s=0.8$, $k_\theta\rho_i=0.4$, $q=1.0$, $\eta_s=3.0$ and $\vartheta_k=0$. As is known from the aforementioned analytical analogy, Fig.4 shows that a series of solutions can exist for Eq.(2). For the weak gradient case ($\epsilon_n=0.5$), we find that the most unstable solution is the ground state (Fig.4a), which is the conventional ballooning structure (Fig.4b). For the strong gradient case ($\epsilon_n=0.2$), the most unstable solution is not the ground state (Fig.4c&d), which corresponds to the unconventional ballooning structure. A detailed analysis of Eq.(2) for present discussion of the unconventional mode structure will be in Ref.[17], which is an extension of Refs.[16, 18].

We have demonstrated that, with strong gradient the most unstable solution can shift from ground state to other non-ground states, which is analogous to the quantum jump between energy levels. Physically, the jump behavior can be understood from the effective potential[16]. The jump happens from one potential well to another, which leads to different energy levels. It is not transparent that the non-ground eigen state in the 1D ballooning space corresponds to the unconventional mode structure in the 2D poloidal plane. Next we confirm this link by showing that the non-ground 2D eigen state solved from Eq.(3) can form the unconventional mode structures observed in the preceding gyrokinetic simulation. The solutions in Refs.[3, 4, 9] are just a weak asymmetric solutions of our series solutions. Almost all the mode structures in Figs.1 and 3 have also been found in the 2D eigen solutions of Eq.(3). Two examples are shown in Fig.5. Therefore, conventional and unconventional series solutions have been found in both 2D eigen solver and GTC initial simulations. The condition for

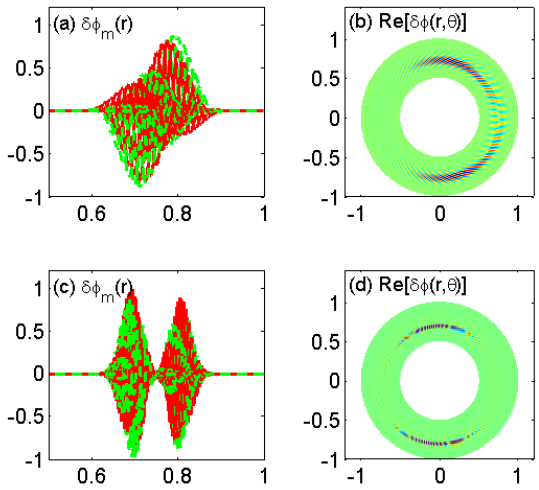

FIG. 5: Typical unconventional mode structures from 2D eigen solution for Eq.(3). (b) is similar to Fig.1(c&d), and (c&d) is similar to Fig.3(d&c)

the jump of the most unstable eigen state to non-ground state is $\epsilon_n < \epsilon_c$, where ϵ_c is a critical gradient parameter which depends on other parameters. In GTC simulations of the HL-2A parameters, the typical critical temperature gradient value is $R_0/L_T = 40 - 120$.

The results from the gyrokinetic simulation and eigen mode analysis show that the unconventional mode structures exist mainly in the strong gradient regime or the H-mode. In the weak gradient regime or L-mode, conventional mode structures still prevail. This can indicate different transport behavior between H-mode and L-mode[19]. In the conventional ballooning structure, the neighboring Fourier modes $u_m \simeq u_{m+1}$, the effective correlation length may be estimated as the width of radial envelope of the modes, say, ΔA. Whereas, in the unconventional ballooning structures, especially for anti-ballooning structure, $u_m \simeq -u_{m+1}$ can occur, i.e., a 180° phase shift for the neighboring Fourier modes, which can change the effective correlation length to the distance of neighboring mode-rational surfaces Δr_s. Considering that $\Delta r_s \ll \Delta A$, we can expect that the H-mode can have better confinement. However, to fully understand these subtle issues, a self-consistent nonlinear gyrokinetic simulation is required.

To summarize, a broad class of unconventional ballooning modes are found for electrostatic drift waves (TEM and ITG) by the gyrokinetic simulation, which is shown to be common in the strong gradient regime. These unconventional mode structures are shown to correspond to the non-ground-state solutions of the eigen mode equation. These results may have important implications for the turbulent transport in tokamaks, i.e., the turbulent transport mechanism in the H-mode can be rather different from that in the L-mode.

Discussions with L. Chen, H. T. Chen and Z. X. Lu are acknowledged. The work was supported by the National Magnetic Confinement Fusion Science Program under Grant Nos. 2015GB110000 and 2013GB111000, the Recruitment Program of Global Youth Experts.

[1] W. Horton, Rev. Mod. Phys., **71**, 735 (1999).
[2] G. Rewoldt, Z. Lin and Y. Idomura, Computer Physics Communications, **177**, 775 (2007).
[3] T. Xie, Y. Z. Zhang, S. M. Mahajan and A. K. Wang, Phys. Plasmas, **19**, 072105 (2012).
[4] D. Dickinson, C. M. Roach, J. M. Skipp and H. R. Wilson, Phys. Plasmas, **21**, 010702 (2014).
[5] J. W. Connor, R. J. Hastie and J. B. Taylor, Phys. Rev. Lett., , **40**, 396 (1978).
[6] J. W. Connor and J. B. Taylor, Phys. Fluids **30**, 3180 (1987).
[7] G. Rewoldt, W. M. Tang and M. S. Chance, Phys. Fluids, **25**, 480 (1982).
[8] J. Q. Dong, L. Chen, F. Zonca and G. D. Jian, Phys. Plasmas, **11**, 997 (2004).
[9] R. Singh, S. Brunner, R. Ganesh and F. Jenko, Phys. Plasmas, **21**, 032115 (2014).
[10] D. P. Fulton, Z. Lin, I. Holod and Y. Xiao, Phys. Plasmas, **21**, 042110 (2014).
[11] Y. Xiao, I. Holod, Z. Wang, Z. Lin and T. Zhang, Phys. Plasmas, **22**, 022516 (2015).
[12] Z. Lin and T. S. Hahm, Phys. Plasmas, **11**, 1099 (2004).
[13] H. S. Xie, Y. Xiao, D. F. Kong and Z. Lin, Gyrokinetic Simulations of the HL-2A Tokamak H-mode Edge Turbulence. I. Electrostatic Physics, to be submitted.
[14] H. S. Xie and Y. Xiao, Phys. Plasmas, **22**, 022518 (2015).
[15] Z. X. Lu, The Complex Mixed WKB-full-wave Approach and Its Application to the 2D Mode Structure Analysis of ITG/CTEM Drift Waves, submitted.
[16] L. Chen and C. Z. Cheng, Phys. Fluids, **23**, 2242 (1980).
[17] H. T. Chen *et al*, to be submitted.
[18] W. Horton, D. Choi and W. M. Tang, Phys. Fluids, **24**, 1077 (1981).
[19] L. Chen, private communications.